Eur. Phys. J. Appl. Phys. **55**, 11201 (2011)
DOI: 10.1051/epjap/2011100294

THE EUROPEAN PHYSICAL JOURNAL APPLIED PHYSICS

Regular Article

Biophysical approach for studying the MinD protein dynamics and energy landscape: a novel use of the spot tracking technique

P. Kanthang[1,2], W. Ngamsaad[2], N. Nuttavut[3], W. Triampo[3,4,5,a], D. Triampo[6,7], and C. Krittanai[8]

[1] Rajamangala University of Technology Phra Nakhon, Bangkok 10800, Thailand
[2] School of Science, University of Phayao, Phayao 56000, Thailand
[3] R&D Group of Biological and Environmental Physics, Department of Physics, Faculty of Science, Mahidol University, Bangkok 10400, Thailand
[4] Institute for Innovative Learning, Mahidol University, 999, Phuttamonthon 4 Road, Salaya, Nakorn Pathom 73170, Thailand
[5] ThEP Center, CHE, 328 Si Ayutthaya Road, Bangkok 10400, Thailand
[6] Department of Mathematics, Faculty of Science, Mahidol University, Bangkok 10400, Thailand
[7] Department of Chemistry, Center of Excellence for Innovation in Chemistry, Faculty of Science, Mahidol University, Rama VI Rd, Bangkok 10400, Thailand
[8] Institute of Molecular Biosciences, Mahidol University, Salaya Campus, Nakhonpathom, Thailand

Received: 25 July 2010 / Received in final form: 31 March 2011 / Accepted: 11 April 2011
Published online: 21 July 2011 –

Abstract. The dynamics of MinD proteins have been acknowledged as playing a central role in accurate cell division. In our study, a spot tracking technique (STT) was applied to track motion and quantitatively characterize the dynamic behavior of MinD proteins on the level of particle cluster in *Escherichia coli*. We focused on the time and spatial distribution of MinD proteins. With the STT technique, the main quantitative results are twofold: (i) dynamic local and global pattern formations and (ii) energy landscape. The overall MinD cluster motion is governed by two dynamical time scales, namely the (slow) trapping time (∼26 s) that appears at the cell poles, and the (fast) switching time (∼1–2 s) which emerges between the cell poles. MinD cluster motion at the polar zones performs subdiffusion. The energy landscape is found to be two wells and one barrier. These energy landscape results are to relate with the memory effect of GFP-MinD cluster motion, measuring the PSD exponent approximately 1.57 ($\alpha \sim 0.57$) corresponding to the estimated potential depth $U_0 \sim 1.75 k_B T$.

1 Introduction

In *Escherichia coli* and other rod-shaped bacteria, cell division depends on the precise placement of a division septum at the middle of the cell, a process initiated by the assembly of an equatorial ring (*Z*-ring) of tubulin-like FtsZ GTPase on the cytoplasmic membrane [1,2]. The *Z*-ring assembly is spatially restricted to the mid-cell by nucleoid occlusion [3,4] and by the dynamics of the Min system [4–6]. The Min system consists of MinC, MinD, and MinE expressed from the *minB* operon [5] which restricts separation to the desired potential division site at mid-cell through the oscillatory cycle from pole to pole (review Ref. [7]).

A number of previous studies of Min protein oscillations focus on spatial-temporal pattern formation and the biochemical basis function [7,8]. However, the experimental data of spatial-temporal pattern formations have been poorly quantitatively interpreted for physical quantities. Recently, the two excellent studies by Loose et al. [9] and Ivanov and Mizuuchi [10] show that MinD and MinE generate self-sustaining waves of membrane association and dissociation over a flat membrane in vitro. Both studies demonstrate spontaneous ATP-dependent dynamic patterning of MinD and MinE on the surface of planar lipid bilayers and that, as predicted by most models, pattern dynamics involves rapid cycling of the proteins on/off the membrane. In addition, Unai et al. quantitatively investigated MinD dynamics on the level of particle cluster. Using a spot tracking technique (STT) [11] – which shares a common feature with single particle tracking [12,13] – they focused on the position and motion of the maximum in the spatial distribution of MinD proteins. STT results quantitatively provide us with information on position alterations and time sequences which can be used to analyze the GFP-MinD dynamics. Globally, MinD proteins perform oscillatory pole-to-pole motion. However, the major characteristics of MinD dynamics are distinguished not only by the trademark oscillatory pattern between the polar zones, but also by the local membrane occupation pattern, or horseshoe structure, in the polar

[a] e-mail: wtriampo@gmail.com

zone [7,14]. Therefore, high concentrations of GFP-MinD are mostly found in the polar regions, and they are believed to correspond to polar zone growth by the formation of MinD polymerization at the cytoplasmic membrane [15,16]. However, several other physical properties of MinD proteins especially in quantitative ways – such as transport properties and energy landscape – are yet to be explored.

In our work, we applied the STT to reveal the underlying spatial-temporal pattern formation dynamics and energy landscape of MinD proteins. We specifically focused on the physical quantities of MinD cluster dynamics, including mean-square displacements (MSDs), time memories, spatial distributions, and effective potential profiles. Moreover, we revealed the relation between potential profiles and diffusion modes.

2 Materials and methods

2.1 Bacterial strain and growth conditions

E. coli RC1/pFX9 [Δmin/P$_{lac}$-*gfp*::Δ*minD* Δ*minE*] was kindly provided by Yu-Ling Shih (Department of Microbiology, University of Connecticut, Health Center) [17]. To culture MinD labeled with green fluorescent proteins (GFP), a starter of RC1/pFX9 cells was grown in LB medium with 50 μg/ml ampicillin, 25% glucose, at 37 °C and shaken overnight at 250 rpm. Then, 1% of the overnight culture was taken to grow in the new medium until the $OD_{600\,nm}$ was approximately 0.4. The centrifugation was performed at 3000 rpm for 15 min to collect the cells. Cells were then re-suspended in the same medium containing 0.1 mM isopropyl-β-D-thiogalactopyranoside (IPTG) for protein induction. The cell culture was diluted with the media used before (see Ref. [11]).

2.2 Image acquisition and spot tracking technique

For fluorescence image sequences, a Zeiss Axioskop 2 microscope and A-plan 100×/1.25 oil lenses were used with InVivo software support, and with exposure times of 900 ms. A charge-coupled device (CCD) camera (Evolution QEi monochrome) was attached to the video port of the microscope to acquire images and movies at 1 frame/s. In our experimental preparation, 5–7 μl of sample was dropped onto a glass slide coated with 5 μl poly-L-lysine (0.1%) and then covered by a coverslip at room temperature before examination.

The spot tracking technique was used to follow the region of interest (ROI) which gave off the highest GFP-MinD concentration signal. This highest intensity signal is the representation of the cluster protein in the cell as shown in Figure 1. A MinD cluster indicates high MinD polymerization. The data obtained from measurements were supported by the SpotTracker Java plug-in for the public domain ImageJ software (for more details, see [11]). This tracking provides the time series data for the position of the ROI of the cluster protein as a text file (x, y coordinates), which detects ROI as a small neighborhood (3 × 3 pixels) as shown in Figure 1c-c"". More details of this tracking as a time algorithm can be found in Sage et al. [18]. The acquired positions were analyzed with MATLAB software to calculate the physical quantities, including: time memory, transport mode, spatial probability density, and energy profile.

2.3 Mean-square displacement and subdiffusion measurement

The time series of their positions denoting $\vec{r}(t) = (x(t), y(t))$ were recorded. Since the overall motion analyzed using all data points of positions was found to be dominated by the motion at the polar zones [11], our main focus was to gain more understanding within the vicinity of the poles. To do so, new data sets were obtained by excluding the data of the protein's position around the mid-cell area, which resulted in leaving only the polar zone data sets to be analyzed. We then calculated the mean-square displacements (MSD), $\left\langle |\Delta\vec{r}|^2 \right\rangle$. The average was taken over time within a single trajectory as follows [12,13,19,20]:

$$MSD(n\Delta t) = \frac{1}{N-1-n}\sum_{i=1}^{N-1-n}\Big\{[x(i\Delta t + n\Delta t) - x(i\Delta t)]^2 + [y(i\Delta t + n\Delta t) - y(i\Delta t)]^2\Big\}, \quad (1)$$

where N is the total number of frames; n is the number of the time interval, which is related to time lag; and i is the positive integer. Theoretically, the MSD of a diffusing particle varies with time as $\left\langle |\Delta\vec{r}(t)|^2 \right\rangle \propto t^{\alpha}$, where the dynamic exponent α distinguishes the type of diffusion encountered; $\alpha = 1$ indicates normal Brownian diffusion; $0 < \alpha < 1$ indicates subdiffusion; and $\alpha > 1$ indicates superdiffusion [12,21–23].

2.4 Power spectrum analysis

The positions of GFP-MinD clusters were visualized in terms of the trajectories on the long axis, as shown in Figure 2b. We analyzed the time memory by using the power spectrum density ($P(f)$) of the long axis coordinates $x(t)$ [22–24]. We followed the Welch method [25] as implemented in MATLAB (see MATLAB documentation for details of the algorithm: http://www.mathworks.com/access/helpdesk/help/toolbox/signal/pwelch.html).

The power spectrum density based on the Fourier transform of the autocorrelation function of position ($P_x(f)$), where $P_x(f) = \left\langle |X(f)|^2 \right\rangle$, and $X(f)$ is the Fourier transform of the coordinate $x(t)$. If the motion of the MinD cluster molecules is described by a generalized Langevin equation, $\alpha = 1$ indicates normal Brownian diffusion and $0 < \alpha < 1$ indicates subdiffusion [22,23,26] in the power law of the power spectrum density $P(f) \sim f^{-(1+\alpha)}$ [24], where the dynamic exponent α distinguishes the type of diffusion encountered.

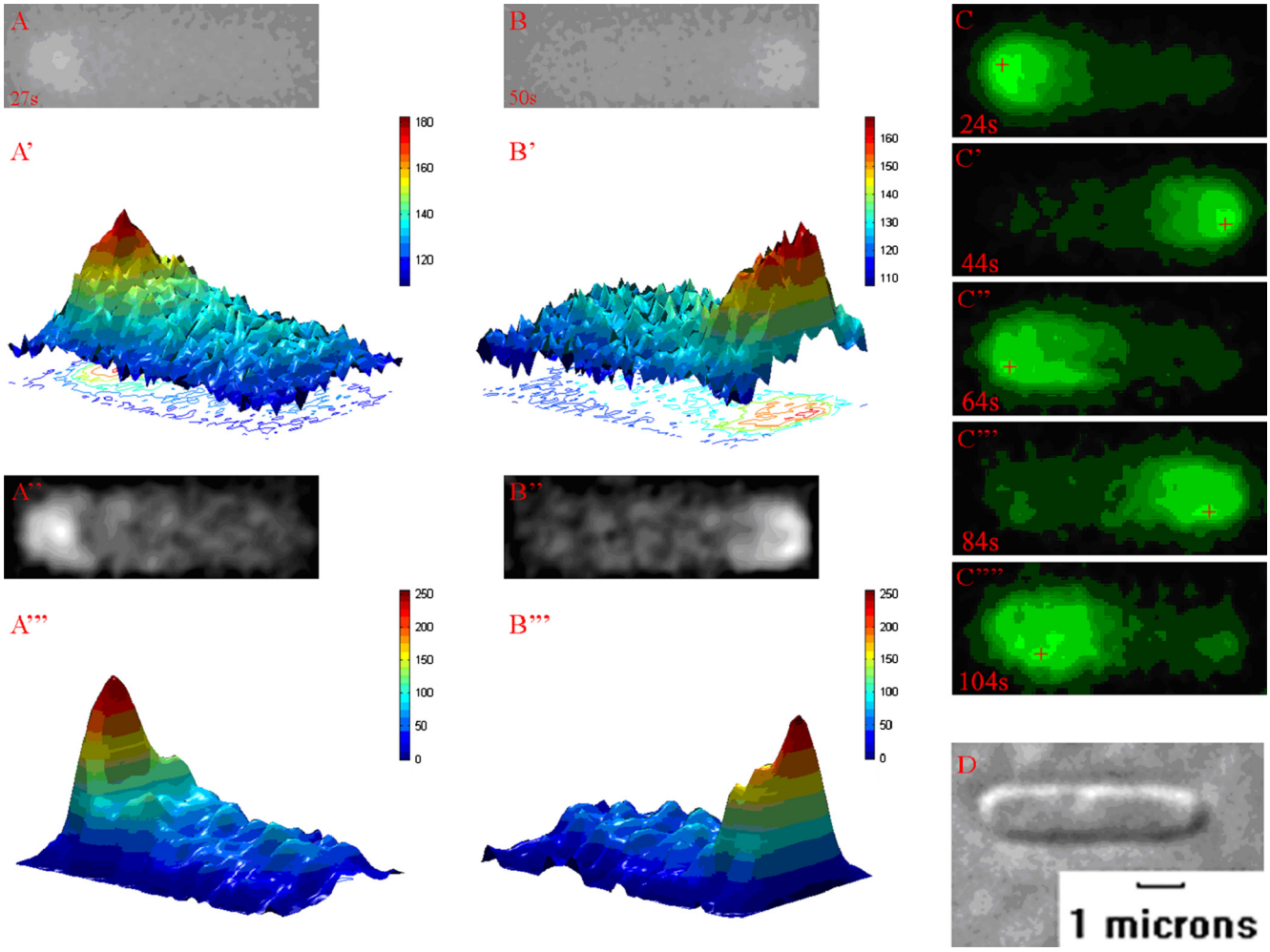

Fig. 1. (Color online) Image processing and SpotTracking results for RC1 *E. coli* cell [*min*/P_{lac}-*gfp::minD minE*]. (a, b) The samples of raw fluorescence images at time of 27 s, and 50 s. (a', b') shows the intensity plot of fluorescence images corresponding to (a, b). The color bar corresponds to the characteristic of image where low intensity and high intensity do not differ significantly. (a", b") Fluorescence images of (a, b) after filtering with Gaussian blur and rescaling. (a"', b"') Intensity plot of images (a", b"). The color scale ranges from 0 to 255. The height intensity region is sharper than (a', b'). (c, c', c", c"', c"") Fluorescence images after tracking with SpotTracker at time of 24 s, 44 s, 64 s, 84 s, and 104 s. The positions of ROI are indicated by red cross sign. (d) A DIC image (gray), cell length ∼5 μm.

2.5 Energy landscape and waiting time distribution

We constructed a histogram of the protein positions along the normalized cell length which indicate where the MinD clusters locate. We calculated the apparent effective potential:

$$U(x) = -k_B T \log(P(x)), \tag{2}$$

where $U(x)$ is the effective potential [20,27,28] and $P(x)$ represents the probability density of MinD cluster molecules, which are calculated from the histogram with small bins (∼3% or 0.03 of normalized cell length). We adopted the approach called Kramers' escape problem. With this approach, we can calculate

$$\psi(\tau_e) \approx \tau_e^{-\left(1+\frac{k_B T}{U_0}\right)}, \tag{3}$$

where the *mean waiting time to escape* (τ_e), k_B and T are the Boltzmann constant and absolute temperature, respectively. We have $\alpha = \frac{k_B T}{U_0}$, where α corresponds with the dynamic exponent for the subdiffusive case $0 < \alpha < 1$ [21,29].

3 Results and discussion

Having performed the STT, we obtained a scattering of the coordinates of the protein cluster in the *E. coli* cell, as shown in Figure 2a. This figure reveals that a characteristic of MinD clusters is that they frequently appear at/near the cell poles, especially near the cytoplasmic membrane. This result corresponds to the previous report [30] which showed the localization of MinD in fixed *E. coli* cells. There, the researchers used anti-MinD antiserum and colloidal gold-labeled second antibody to study

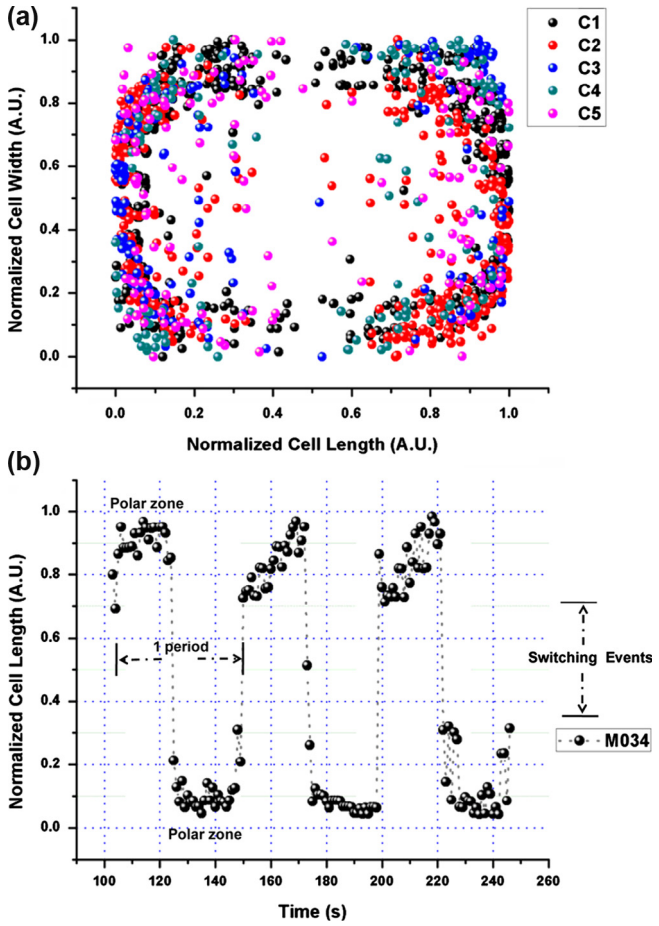

Fig. 2. (Color online) The oscillation pattern and position scattering for GFP-MinD protein cluster. (a) The scattering plot for GFP-MinD cluster along the normalized cell length and cell width. (b) An example of the trajectory of a GFP-MinD cluster.

the membrane-associated protein of MinD via immunoelectron microscopy. This pointed to an explanation relating to the MinD polymerization mechanism [16,31,32]. Figure 2b demonstrates the oscillation pattern of MinD between the cell poles with a period approximately 54.8 ± 8.6 s. This period corresponds to the previous reports, as summarized in Table 1. The overall MinD cluster motion is governed by two dynamical time scales, namely the (slow) trapping time (∼26 s) that appears at the cell poles, and the (fast) switching time (∼1–2 s) which emerges between the cell poles. These phenomena may reflect two different protein mechanisms and time scales. The trapping time concerns MinD polymerization, while the switching time signifies the MinD accumulation at the next pole after depolymerization.

For MSD analysis, we compared the MSD of MinD cluster motion between the trajectory throughout the cell and exclusively at the polar zone. The MSD was found to be significant in characteristic pattern and in the difference expressed by the dynamic exponent α, as shown in Figure 3a. For the MSD throughout the cell $\alpha \sim 0.93 \pm 0.09$ and $R^2 = 0.99$; for the MSD exclusively at the polar zone $\alpha \sim 0.33 \pm 0.18$ and $R^2 = 0.98$. When we compared these dynamic exponents with that of a Brownian simulation where $\alpha \sim 1.01 \pm 0.02$ ($R^2 = 0.99$), it suggested that the cluster motion throughout the cell had the equivalent feature of Brownian motion, while MinD cluster motion exclusively near the polar zones differs from it. The difference between dynamic exponents could result from a difference in characteristic time scale between the two areas as well. We interpreted that MinD cluster motion at the polar zones performs subdiffusion at a time scale of approximately 22 s mostly in the vicinity of polar areas. This time scale is more or less the MinD cluster's half oscillation period, which is referred to as the trapping time. This trapping time could be interpreted as the memory effect (the temporal correlations in a particle's motion that are described in terms of the broad distribution of cage times) of MinD cluster motion at the polar zones, which is believed to arise biologically from its polymerization mechanism [16]. In Figure 3b, to have more understanding about mentioned subdiffusive dynamics, we worked out the time memory of protein cluster dynamics using power spectrum distribution (PSD) analysis. Considering the PSD throughout the cell, we found that $\nu = 1.57 \pm 0.18$ ($\alpha \sim 0.57$) and $R^2 = 0.98$, while exclusively around the polar zone the PSD was found to be $\nu = 1.3 \pm 0.16$ ($\alpha \sim 0.30$) and $R^2 = 0.98$. We compared this characteristic with that of Brownian motion and found that the PSD exponent of Brownian motion was $\nu = 1.91 \pm 0.04$ ($\alpha \sim 0.91$) and $R^2 = 0.96$, which indicates a short-range correlated random process. Hence the PSD exponents of MinD cluster motion imply the memory effect and the power-law correlation, possibly due to the interaction during the trapping time period. As previously pointed out, here the different dynamic exponents of protein cluster motion throughout the cell, and their exclusivity, were once again confirmed. Because the switching events occurred during a very short time compared to the protein cluster dynamics at the polar zones, the switching events did not influence substantially the overall motion. Our findings may be related to the evidence of subdiffusion in *E. coli* cells shown in Golding and Cox's work [23]. They found that subdiffusion in the bacterial cell is independent of the main cytoskeletal elements and is more likely explained by the extremely crowded environment of the cytoplasm. Due to the nucleation and assembly of MinD, the subdiffusive motion may be described via the membrane association of MinD which is mediated by a C-terminal membrane-targeting sequence (MTS) [31,33]. This process possibly can target the MinD protein to lipid bilayers by the electrostatic attraction of its positively charged amino acids with the anionic lipid-enriched domain [16,32,34,35]. According to this characteristic function of MinD protein, the GFP-MinD cluster motion will be trapped on the membrane surface which induced the distribution of cage times and lead to anomalous subdiffusion.

In terms of energy landscape, we began by analyzing the protein cluster distribution along the normalized cell

Table 1. Some physical quantities of MinD proteins.

Physical quantities	MinD key finding	References
Oscillation periods	∼55 s	Hale et al. [43]
	∼40 s	Raskin and de Boer [42]
	∼60 s	Shih et al. [17]
	∼55 s	Unai et al. [11]
Cluster velocities	Polar zones ∼0.3 μm/s	Unai et al. [11]
	Pole to pole ∼3 μm/s	Unai et al. [11]
Diffusion coefficients	Cytoplasmic diffusion ∼17 $\mu m^2/s$	Meacci et al. [47]^{FCS}
	Cytoplasmic membrane ∼0.2 $\mu m^2/s$	Meacci et al. [47]^{FCS}
	Polar zones ∼0.3 $\mu m^2/s^{\alpha}$	Unai et al. [11] ^{STT}

FCS: Fluorescence Correlation Spectroscopy.
STT: Spot Tracking Technique.

length of individual cells, as shown in Figure 4a. This figure has the same feature as the scattering plot in Figure 2a, where the MinD cluster is highly distributed near the polar zones. In the same way, we found the spatial distribution of MinD cluster dynamics for several cells (13 cell samples), as shown in Figure 4b. Each point on the graph was evaluated from the mean value of bin centers along the normalized cell length. We fitted this data set with a double Gaussian function, which was based on the assumption of normal distribution at the cell poles. The fitting functions follow previous experiments and theoretical studies for FtsZ MinD and MinE proteins [11,17,36–40]. Their results led us to predict the possible division site of an *E. coli* cell that occurs in the region where MinD has minimum spatial distribution and appears mostly near the mid-cell zone [11,40–43]. According to the spatial distribution of MinD cluster dynamics, we could evaluate the effective potential for individual cluster molecules, as shown in Figures 4c and 4d. From these evaluations, information about physical, force-producing mechanisms responsible for diffusive motion of MinD should be contained in STT trajectories, without the need to apply external forces. MinD cluster dynamics perform the bistable, or double-well, potential profile. The minimum regions represent the potential depths that occur near the polar zones. The potential barrier region appears at the mid-cell zone. This potential profile is well known for describing the generating oscillation pattern between two metastable zones [44]. Not surprisingly, the effective potential curves were not smooth and symmetrical. These issues are clearly reflected via the individual effective apparent potentials, as shown in Figure 4c. The distribution of the small well depths along the relative cell length seems to reflect the valley model [45,46], which may not only perform characteristic trapping events for individual cells, but also different correlated motions on the relative space. In terms of the average effective potential feature shown in Figure 4d, we checked potential characteristics via the fitting curve with the higher order of potential function, which shows that asymmetry terms are not equal to zero. This case indicated via probability density that cluster MinD concentrated in different regions of the *E. coli* cell, such as at ∼30%, ∼75%, and ∼80% of cell length. This situation may suggest some interaction between the MinD cluster and the cytosol or membrane. We analyzed the relation between the waiting time distribution and the effective potential by using the Kramers' escape problem. We found that the dynamic exponent α related to the potential depths where $\alpha = k_BT/U_0$. We also found that the average potential depth from the experimental data is $U_0 \sim 1.68k_BT$, which relates to the dynamic exponent $\alpha \sim 0.6$. The curve fitting of the double-well potential ($y = -ax^2 + bx^4$) indicated an estimated potential depth of $U_0 \sim 1.46k_BT$ (13% error), with the dynamic exponent $\alpha \sim 0.69$ (15% error). Moreover, we found the effective potential data by considering the dynamics throughout the cell in relation to the PSD exponent shown in Figure 3b. The result corresponded to the memory effect of GFP-MinD cluster motion, with the PSD exponent approximately 1.57 ($\alpha \sim 0.57$) which corresponded to the estimated potential depth $U_0 \sim 1.75k_BT$. When we considered the dynamics locally at the polar zones or trapping event zones which corresponded to the average dynamics over half of the effective potential shown in Figure 4d, the dynamic exponent measured approximately 0.33, with the escape potential approximately $3k_BT$. When comparing these results to the mean dynamic exponent of MSD and PSD at the polar zone, as shown in Figures 3a and 3b, this may indicate that at local polar zone MinD "see" the barrier almost twice higher than that of globally throughout the cell. Because MinD cluster dynamics have different dynamical time scales, especially at the polar zone and mid-cell, the latter region is relatively small time scale (∼10 folds), as shown in Table 1. This led us to separate the effective potential into two zones: one at the polar region and the other with a barrier at the mid-cell. Because the energy landscape had two wells and one barrier, we described the behavior of MinD cluster near mid-cell by using activation over the energy barrier. We assumed that the flight events that occurred between the trapping events were driven by thermal energy (more than $\sim 1.6k_BT$). The thermal energy means the effective energy for driving the GFP-MinD cluster motion. At this region, it was guaranteed that the cluster protein performed in

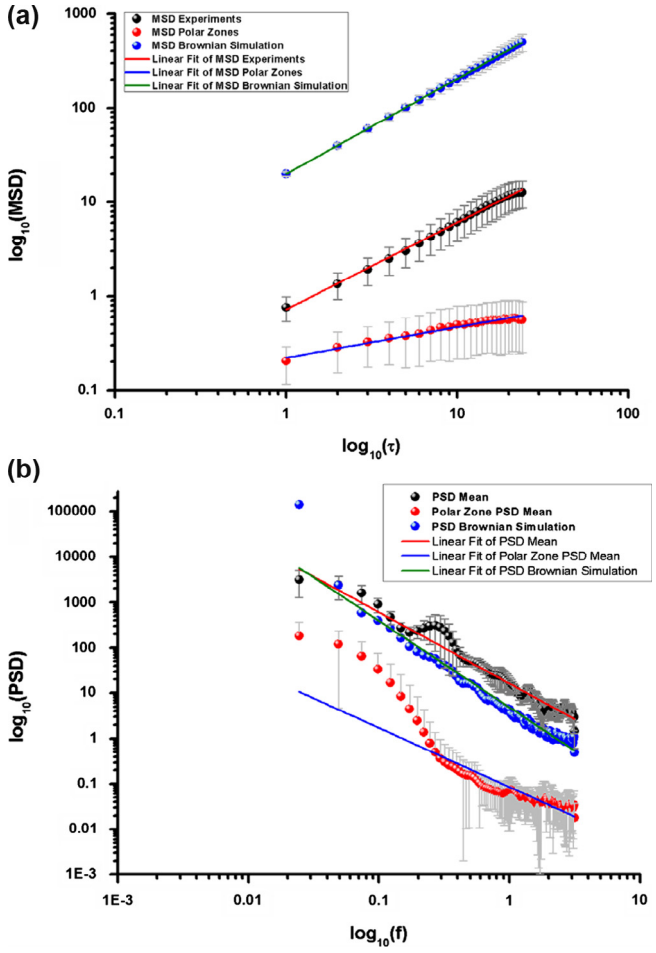

Fig. 3. (Color online) The diffusive motion and time memory for GFP-MinD protein cluster motion. (a) The log-log plot of MSDs for the trajectory throughout the cell and the trajectory at the polar zone. Black spots represent the mean value of MSDs throughout the cell. Red line indicates the linear curve fitting with a slope approximately 0.93 ± 0.097 and $R^2 = 0.998$. Red spots indicate the mean value of MSDs at the polar zones. Blue line indicates the linear curve fitting with a slope approximately 0.33 ± 0.167 and $R^2 = 0.98$. Blue spots indicate the mean value of MSDs from the Brownian motion simulation. Green line indicates the linear curve fitting with a slope approximately 1.01 ± 0.02 and $R^2 = 0.99998$ (50 simulations). (b) The power spectrum density (PSD) of GFP-MinD cluster trajectories that follow the trajectory data sets in Figure 2a. Black spots represent the mean value of PSDs throughout the cell. Red line indicates the linear curve fitting with a slope approximately 1.57 ± 0.04 ($R^2 = 0.98$). Red spots indicate the mean value of PSDs at the polar zones. Blue line indicates the linear curve fitting with a slope approximately 1.3 ± 0.16 ($R^2 = 0.83$). Blue spots indicate the mean value of PSDs from the Brownian motion simulation. Green line indicates the linear curve fitting with a slope approximately 1.91 ± 0.04 and $R^2 = 0.96$ (50 simulations).

an unstable mode. The influences of topology specify the function of MinE. This function of MinE gives site specificity to the MinCD division inhibitor, preventing it from blocking division at the proper mid-cell site, while permitting it to prevent separation at other sites [7,9,43,44]. Hence the probability density of the GFP-MinD cluster was lowest at mid-cell (∼50% of cell length), as shown in Figure 4b. At the polar zone, the energy of the GFP-MinD cluster had less energy than the other region. The cluster protein performed in stable mode, which has a high probability density at these regions (∼0% and ∼100% of cell length). This case is consistent with the polar zone assembly. MinD-ATP associates with the inner surface of the cytoplasmic membrane [14,30,31] and polymerizes by lateral diffusion and interaction with other membrane-associated MinD-ATP molecules, giving rise to the polar zone [7]. Under structure analysis, MinD is also known to behave like a motor protein, which has ATPase activity. MinD contains a deviant Walker box ATP-binding site and is an ATPase [8]. From the energy profile of MinD, we see that cluster molecules are not only related to subdiffusive motion, but also to performed prediction of the division site near the mid-cell.

We would like to highlight that the underlining quantitative characterization is that with the STT technique the main quantitative results (based on dynamic local and global pattern formation considerations via mean-square displacement, power spectrum and energy landscape) provide consistent results. This is to say that even if we disregard the energy landscape analysis, our conclusion is still valid, as can be seen in discussion part of this paper, where we make comparisons and connections with the results of other authors. However, it is our view that the physics audience benefits more by casting the results in terms of potential landscape. To be specific, this system of proteins should be considered as equilibrium statistical thermodynamics for a given constant temperature ($T = 25\,^{\circ}\mathrm{C}$). To us this is then an issue of equilibrium statistical thermodynamics vs. non-equilibrium statistical thermodynamics. It is known that the familiar Gibbs-Boltzmann framework fails in the task of predicting macroscopic behaviors from microscopic information for non-equilibrium systems, unlike when working with its equilibrium counterpart. One of the key properties associated with non-equilibrium behavior is the violation of fluctuation-dissipation theorem (FDT violation). The fluctuation-dissipation theorem relies on the assumption that the response of a system in thermodynamic equilibrium to a small applied force is the same as its response to a spontaneous fluctuation. Therefore, there is a direct relation between the fluctuation properties of the thermodynamic system and its linear response properties. Due to the dissipation of energy (ATP), we believe that the cell has its own mechanism (e.g., metabolism) to supply energy to the cell for

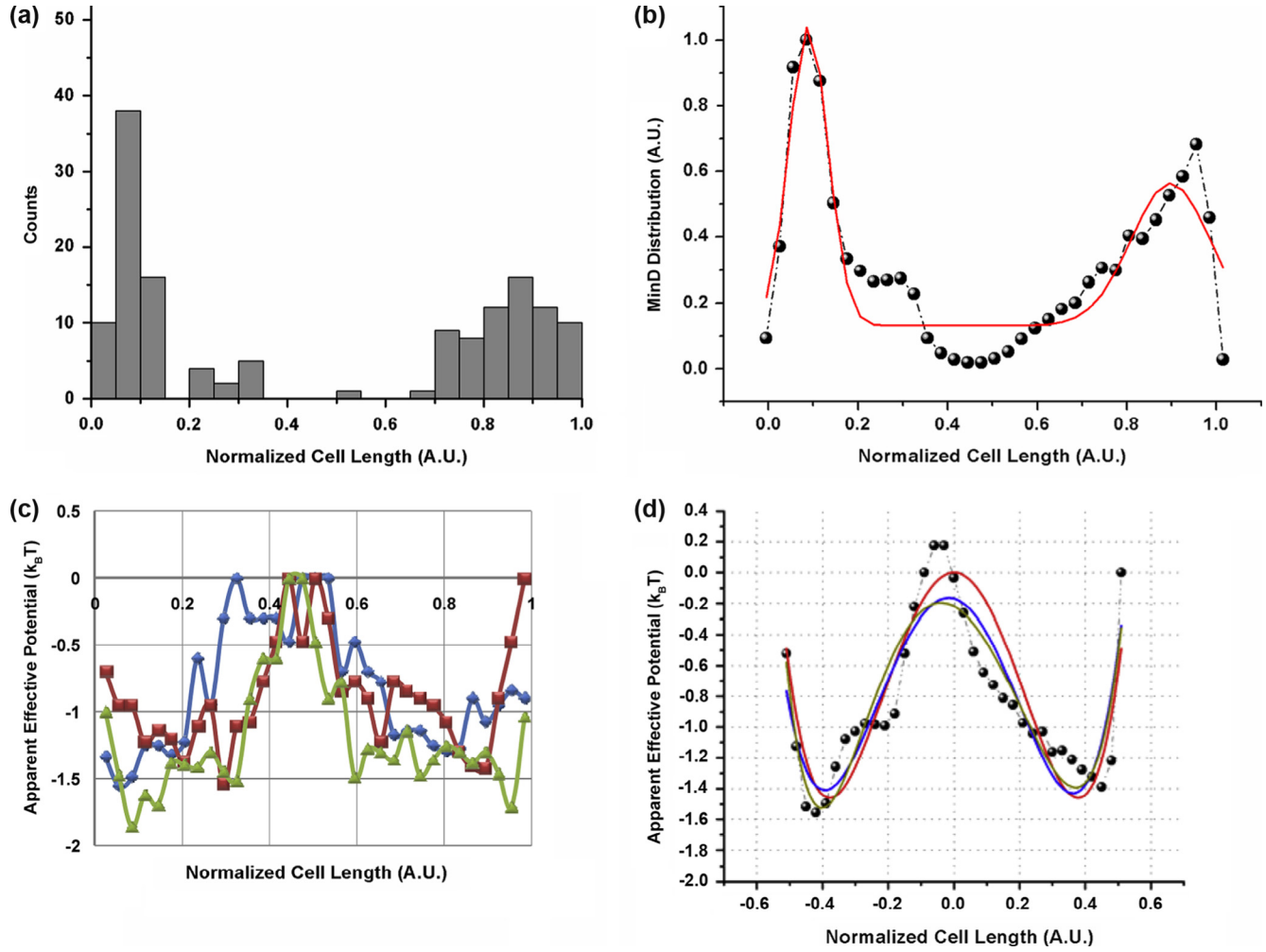

Fig. 4. (Color online) The GFP-MinD cluster distributions and effective potential profiles along the normalized cell length. (a) A typical example of the localization of GFP-MinD cluster (same data set as in Fig. 1b). The distribution of protein cluster is lowest near the mid-cell zone and highest near the polar zones. (b) The MinD distribution along the normalized cell length. The red line indicates the fitting curve of double Gaussian function ($R^2 \sim 0.85$). (c) Examples of the apparent effective (trapping) potential profiles for GFP-MinD cluster. (d) Black spots show the average apparent effective (trapping) potential in experimental data (same data set as in Fig. 3b). Red line represents the double-well potential fitting function ($y = -ax^2 + bx^4$; $R^2 \sim 0.79$). Blue and dark yellow lines represent the expansion term of potential fitting function, in the order: 4 ($y = -a - bx - cx^2 + dx^3 + ex^4$; $R^2 \sim 0.78$) and 6 ($y = -a - bx - cx^2 + dx^3 + ex^4 - fx^5 + gx^6$; $R^2 \sim 0.78$), respectively.

its functioning. Therefore, energy fluctuation could occur without losing equilibrium, as long as the temperature is kept constant. We thus can consider the *E. coli* system as a canonical ensemble or grand canonical ensemble to find the macroscopic property of *equilibrium thermodynamics*. We would like to clarify more about ATP, the mechanism of MinD protein movement dynamics (reaction-diffusion-like motion) which requires the ATP-consuming process especially in terms of the polymerization on the cytoplasmic membranes This mechanism most likely occurs at/near the polar zones. Also the associated hydrolysis process from MinE protein, in terms of E-ring structure, activates the MinD-ATP, leading to conversion of ATP to ADP on the cytoplasmic membrane (from mid-cell to polar zone), MinD-ADP after hydrolysis is released from the cytoplasmic membrane. This process results in the site-specific function of MinE proteins that prefer MinE proteins to localize around the mid-cell zone. These result in the organization of MinD proteins to concentrate or trap at the polar zones.

4 Concluding remarks

In conclusion, an STT was used here to track the maximum distribution of a particle ensemble. The main results were the quantitatively analyzed dynamic pattern formation and energy landscape. The STT can provide accurate enough predictions to suggest useful biological features in predicting protein localization. With improvements in STTs, through data acquisition and data analysis, the STT could become a very well-accepted technique.

It is reasonable to say that this quantitative information could contribute to improvements in the dynamic model of protein oscillation.

The authors thank Mr. D. Blyler for reading the manuscript and comments. Technical assistance by Somruthai Kidsanguan is acknowledged. This research project is supported by Faculty of Science, Mahidol University, the Thailand Research Fund (TRF), the Commission on Higher Education, Ministry of Education, Mahidol University Research Grant, Center of Excellence for Innovation in Chemistry (PERCH-CIC), and the Thailand Center of Excellence in Physics (ThEP).

References

1. J. Lutkenhaus, S.G. Addinall, Annu. Rev. Biochem. **66**, 93 (1997)
2. L.I. Rothfield, S. Justice, J. Garcia-Lara, Annu. Rev. Genet. **33**, 423 (1999)
3. C.L. Woldringh, E. Mulder, P.G. Huls, N. Vischer, Res. Microbiol. **142**, 309 (1991)
4. X.C. Yu, W. Margolin, Mol. Microbiol. **32**, 315 (1999)
5. P.A.J. de Boer, R.E. Crossley, L.I. Rothfield, Cell **56**, 641 (1989)
6. L.I. Rothfield, Y.-L. Shih, G. King, Cell **106**, 13 (2001)
7. L.I. Rothfield, A. Taghbalout, Y.-L. Shih, Nat. Rev. Microbiol. **31**, 959 (2005)
8. Y.-L. Shih, L.I. Rothfield, Microbiol. Mol. Biol. Rev. **70**, 729 (2006)
9. M. Loose, E. Fischer-Friedrich, J. Ries, K. Kruse, P. Schwille, Science 320, **789** (2008)
10. V. Ivanov, K. Mizuuchi, Proc. Natl. Acad. Sci. USA **107**, 8071 (2010)
11. S. Unai, P. Kanthang, U. Junthon, W. Ngamsaad, W. Triampo, C. Modchang, C. Krittanai, Biologia **64**, 27 (2009)
12. M.J. Saxton, K. Jacobson, Annu. Rev. Biophys. Biomol. Struct. **26**, 373 (1997)
13. H. Qian, M. Scheetz, E.L. Elson, Biophys. J. **60**, 910 (1991)
14. S.L. Rowland, X. Fu, M.A. Sayed, Y. Zhang, W.R. Cook, L. Rothfield, J. Bacteriol. **182**, 613 (2000)
15. Z. Hu, J. Lutkenhaus, Mol. Cell **7**, 1337 (2001)
16. K. Suefuji, R. Valluzzi, D. RayChaudhuri, Proc. Natl. Acad. Sci. USA **99**, 16776 (2002)
17. Y.-L. Shih, T. Le, L. Rothfield, Proc. Natl. Acad. Sci. USA **100**, 7865 (2003)
18. D. Sage, F.R. Neumann, F. Hediger, S.M. Gasser, M. Unser, IEEE Trans. Image Process. **14**, 1372 (2005)
19. K. Suzuki, K. Ritchie, E. Kajikawa, T. Fujiwara, A. Kusumi, Biophys. J. **88**, 3659 (2005)
20. S. Jin, P.M. Haggie, A.S. Verkman, Biophys. J. **93**, 1079 (2007)
21. R. Metzler, J. Klafter, Phys. Rep. **339**, 1 (2000)
22. I.M. Tolic-Nørrelykke, E.-L. Munteanu, G. Thon, Phys. Rev. Lett. **93**, 078102 (2004)
23. I. Golding, E.C. Cox, Phys. Rev. Lett. **96**, 098102 (2006)
24. R.N. Mantegna, H.E. Stanley, *An Introduction to Econophysics Correlations and Complexity in Finance*, (Cambridge University Press, Cambridge, UK, 2000)
25. P.D. Welch, IEEE Trans. Audio Electroacoust. **AU-15**, 70 (1967)
26. G.R. Kneller, K. Hinsen, J. Chem. Phys. **121**, 10278 (2004)
27. K. Ritchie, X.-Y. Shan, J. Kondo, K. Iwasawa, T. Fujiwara, A. Kusumi, Biophys. J. **88**, 2266 (2005)
28. F. Daumas, N. Destainville, C. Millot, A. Lopez, D. Dean, L. Salome, Biophys. J. **84**, 356 (2003)
29. I.Y. Wong, M.L. Gardel, D.R. Reichman, E.R. Weeks, M.T. Valentine, A.R. Bausch, D.A. Weitz, Phys. Rev. Lett. **92**, 178101 (2004)
30. P.A.J. de Boer, R.E. Crossley, L.I. Rothfield, EMBO J. **10**, 4371 (1991)
31. T.H. Szeto, S.L. Rowland, L.I. Rothfield, G.F. King, Proc. Natl. Acad. Sci. USA **99**, 15693 (2002)
32. Z. Hu, E.P. Gogol, J. Lutkenhaus, Proc. Natl. Acad. Sci. USA **99**, 6761 (2002)
33. Z. Hu, J. Lutkenhaus, Mol. Microbiol. **47**, 345 (2003)
34. E. Mileykovskaya, I. Fishov, X. Fu, B. Corbin, W. Margolin, W. Dowhan, J. Biol. Chem. **278**, 22193 (2003)
35. A. Taghbalout, L. Ma, L. Rothfield, J. Bacteriol. **188**, 2993 (2006)
36. L. Niu, J. Yu, Biophys. J. **95**, 2009 (2008)
37. U. Junthorn, S. Unai, P. Kanthang, W. Ngamsaad, C. Modchang, W. Triampo, C. Krittanai, D. Triampo, J. Korean Phys. Soc. **52**, 639 (2008)
38. M. Howard, A.D. Rutenberg, S. de Vet, Phys. Rev. Lett. **87**, 278102 (2001)
39. K.C. Huang, Y. Meir, N.S. Wingreen, Proc. Natl. Acad. Sci. USA **100**, 12724 (2003)
40. R.V. Kulkarni, K.C. Huang, M. Kloster, N.S. Wingreen, Phys. Rev. Lett. **93**, 228103 (2004)
41. Z. Hu, J. Lutkenhaus, Mol. Microbiol. **34**, 82 (1999)
42. D.M. Raskin, P.A.J. de Boer, J. Bacteriol. **181**, 6419 (1999)
43. C.A. Hale, H. Meinhardt, P.A.J. de Boer, EMBO J. **20**, 1563 (2001)
44. D.M. Raskin, P.A.J. de Boer, Cell **91**, 685 (1997)
45. M.J. Saxton, Biophys. J. **70**, 1250 (1996)
46. H. Haken, *Synergetics, An Introduction. Nonequilibrium Phase-Transitions and Self-Organization in Physics, Chemistry and Biology* (Springer-Verlag, Berlin, Heidelberg, 1977)
47. G. Meacci, J. Ries, E. Fischer-Friedrich, N. Kahya, P. Schwille, K. Kruse, Phys. Biol. **3**, 255 (2006)